The Generalized Quadrature Method of Moments

Rodney O. Fox, Frédérique Laurent, Alberto Passalacqua

The Generalized Quadrature Method of Moments

Rodney O. Fox[a,*], Frédérique Laurent[b], Alberto Passalacqua[c]

[a]*Department of Chemical and Biological Engineering, Iowa State University, 618 Bissell Road, Ames, IA 50011-1098, USA*
[b]*Laboratoire EM2C & Fédération de Mathématiques de CentraleSupélec, CNRS, CentraleSupélec, Université Paris-Saclay, 3 rue Joliot-Curie, 91192 Gif-sur-Yvette, France*
[c]*Department of Mechanical Engineering, Iowa State University, 62529 Union Drive, Ames, IA 50011-2030, USA*

Abstract

The quadrature method of moments (QMOM) for a one-dimensional (1-D) population balance equation was introduced by R. McGraw (Aerosol Science and Technology, **27**, 255-265, 1997) to close the moment source terms. QMOM is defined based on the properties of the monic orthogonal polynomials Q_i of degrees $i = 0, 1, \ldots, n$ that are uniquely defined by the set of $2n$ moments up to order $2n-1$. The moment of order $2n$ is fixed to the boundary of moment space such that the distribution function is approximated by a sum of n Dirac delta functions. Using the recursion coefficients of the orthogonal polynomials for $i > n \geq 1$, the generalized quadrature method of moments (GQMOM) extends the quadrature representation to a sum of $N > n$ terms using the same moments as QMOM. In doing so, the known moments are preserved and higher-order moments correspond to a distribution function in the interior of moment space. Here, GQMOM closures for distributions on $\mathbb{R}$, $\mathbb{R}^+$, and $(0, 1)$ are defined and analyzed. Generally speaking, GQMOM provides a more accurate moment closure than QMOM without increasing the number of moments and at nearly the same computational cost.

Keywords: population balance equation, quadrature-based moment methods, moment closures

1. Introduction

The quadrature method of moments (QMOM) (McGraw, 1997) is arguably the most successful and widely used closure for finding the lower-order moments of the number density function (NDF) found from a one-dimensional (1-D) population balance equation (PBE). There are numerous publications in the scientific literature demonstrating its accuracy for treating particle growth, aggregation and breakage processes. In many applications, only a relatively small number of integral moments are needed to attain sufficient accuracy for representing the properties and evolution of aerosols (McGraw et al., 1998). This is because realistic growth, aggregation and breakage kernels are relatively smooth functions of the particle size, which is a necessary condition for the Gaussian-quadrature approximation of integrals with respect to the NDF to be accurate (Grosch et al., 2007). For example, most aerosol dynamics problems can be treated accurately with between three to five quadrature nodes using QMOM (Marchisio and Fox, 2013; McGraw, 1997), which corresponds to six to ten moments. In this work, we use the 'standard' moments written as integer powers of the phase-space variable. It is also possible to use generalized moments (Grosch et al., 2007; Lage, 2011); however, the limitations associated with the QMOM that we wish to address remain the same (Grosch et al., 2007).

Despite its many successes, the QMOM has an obvious shortcoming, i.e., in order to increase the number of quadrature nodes, one must solve for a larger number of moments. In comparison, closures based on

*Corresponding author
Email addresses: rofox@iastate.edu (Rodney O. Fox), frederique.laurent@ecp.fr (Frédérique Laurent), albertop@iastate.edu (Alberto Passalacqua)

reconstructing the NDF from a fixed set of moments do not suffer from this problem. For example, entropy maximization (EM) (Jaynes, 1957; Mead and Papanicolaou, 1984) provides a closed form for the NDF that can be integrated to arbitrary accuracy when evaluating the moment governing equations found from the PBE. In other words, if a closed form for the NDF (e.g., exponential, lognormal, etc.) is available, then the connection between the number of moments and the number of quadrature nodes is severed, and the overall accuracy of the closure is then controlled by the number of moments. Nonetheless, applying EM with a large number of moments is computationally prohibitive compared to QMOM. Therefore, alternative methods with the computational simplicity of QMOM, but with the accuracy of EM are needed. In any case, the number of moments used in QMOM cannot be increased indefinitely. In practice, the moment-inversion algorithm suffers from ill-conditioning (Gautschi, 2004; Grosch et al., 2007; Wheeler, 1974), so that practical applications cannot use more than fourteen to twenty moments.

As we describe in section 2, QMOM corresponds to a *particular* reconstruction of the NDF for the given set of integral moments. As discussed in McGraw et al. (1998) for isomomental NDF, the reconstruction is not unique even when the number of known integral moments is infinite. Compared to the NDF from EM, the QMOM NDF produces the smallest possible value for the next (unknown) even-order moment. Theoretically, there exists an infinite number of NDF with the same (known) moments used in EM and QMOM. Thus, the problem reduces to choosing one such NDF in a computationally efficient manner. For example, with an efficient algorithm, we should be able to find the Gaussian quadrature that corresponds to the chosen NDF with the same algorithm employed with QMOM. In prior work (Yuan et al., 2012), we introduced the extended quadrature method of moments (EQMOM) to achieve this goal. The basic idea behind EQMOM is to reconstruct the NDF using a sum of kernel density functions (KDF) centered around different sizes, but with the same standard deviation σ. One additional (even-order) moment is needed to determine σ using an iterative, 1-D, root-finding procedure. Compared to EM, the dual-quadrature algorithm for EQMOM is very efficient, and the quadrature nodes are easily found for the known KDF (Gautschi, 2004; Lage, 2011). EQMOM has been widely used in the literature, and various extensions have been proposed, e.g., using different definitions for the KDF (Madadi-Kandjani and Passalacqua, 2015; Pigou et al., 2018). Nonetheless, it is not always possible to find a value for σ that yields the additional moment and, even when such a σ exists, the iterative process needed for EQMOM is not as fast as QMOM. Moreover, the full set of N abscissae found from the individual KDF do not correspond to N zeros of an orthogonal polynomial of degree N. Thus, EQMOM is ill-conditioned when combined with the conditional quadrature method of moments (CQMOM) used for treating bi-variate distributions (Yuan and Fox, 2011).

In this work, we propose a generalized version of QMOM (GQMOM) that overcomes all of the above-mentioned shortcomings of QMOM and EQMOM. The key technical point employed in GQMOM is the three-term recurrence relation for the family of orthogonal polynomials corresponding to the reconstructed NDF. In short, instead of attempting to specify the unknown moments of the NDF (which is extremely difficult, if not impossible), we choose an NDF with an allowable set of recurrence coefficients. Interestingly, high-order moment-bounds approximations that arise in seemingly unrelated problems are treated in a similar manner (McGraw and Merry, 1985). In section 2.2, we discuss how the recurrence coefficients are related uniquely to the moments, and in section 3 we define closures for the GQMOM recurrence coefficients for NDF defined on $\mathbb{R}$, $\mathbb{R}^+$, and $(0,1)$ based on well-known NDF (e.g., Gaussian, gamma, lognormal, beta). However, these closures are not unique and the reader can easily compose choices with other desired properties. Once the recurrence coefficients are fixed, the Gaussian quadrature can be computed immediately for an arbitrarily large number of nodes (Gautschi, 2004; Wheeler, 1974). In this manner, we do not need the explicit functional form for the NDF, but rather we determine the NDF implicitly through knowledge of its recurrence coefficients. In practice, an approximation of the NDF is available through the weights and abscissae of the Gaussian quadrature by setting their number to be sufficiently large. In summary, given its facile implementation in PBE solvers based on QMOM, we expect that GQMOM will become the method of choice for solving moment systems derived from a 1-D PBE.

The remainder of this work is arranged as follows. In section 2 we provide a brief overview of QMOM in the context of a 1-D, time-dependent PBE with emphasis on its relationship to orthogonal polynomials and realizable moments. In section 3 we define GQMOM for NDF defined on $\mathbb{R}$, $\mathbb{R}^+$, and $(0,1)$, and show some simple examples of the resulting quadrature. By a change of variables, any NDF defined on a semi-

infinite or finite interval can be mapped to $\mathbb{R}^+$ or $(0,1)$, respectively. Therefore, these three definitions of GQMOM cover almost all situations arising in applications. In general, GQMOM is equivalent to QMOM for applications where QMOM works well. Thus, in section 4, we evaluate the performance of GQMOM for some difficult test cases for which QMOM does not yield satisfactory results. Generally speaking, in the context of a 1-D PBE, GQMOM provides the same advantages as EQMOM and EM, but at a lower computational cost. Examples comparing the different methods for some difficult cases are also provided in section 4.

2. QMOM for the resolution of a 1-D PBE

Here we provide a brief overview of QMOM for a spatially homogeneous, 1-D PBE. Application to spatially inhomogeneous cases is described in detail in Marchisio and Fox (2013).

2.1. Principle of the method

The key principle of QMOM is to close moment equations derived from a PBE by using a Gauss quadrature for the source terms (McGraw, 1997). Let $f(t,\xi)$ be the NDF for the phase-space variable $\xi \in \mathbb{B} \subseteq \mathbb{R}$ at time $t \in \mathbb{R}^+$ with initial condition $f(t,\xi) = f_0(\xi)$. For clarity, in this work the set $\mathbb{B}$ will be either $\mathbb{R}$, $\mathbb{R}^+$, or the interval $(0,1)$. To illustrate QMOM, hereinafter we assume that $f(t,\xi)$ is governed by a PBE with nonlinear source terms (see examples in section 4):

$$\partial_t f = S(t,\xi). \tag{1}$$

In general, $S(t,\xi)$ will be a functional of $f(t,\xi)$ and its moments (Marchisio and Fox, 2013). The kth integral moment of the NDF is

$$M_k(t) = \int_{\mathbb{B}} \xi^k f(t,\xi)\,\mathrm{d}\xi \tag{2}$$

for $k \in \mathbb{N}$. Let $\mathbf{M}_{2n-1} := (M_0, M_1, \ldots, M_{2n-1})$ be the moment vector of length $2n$ with $n \in \mathbb{N}$.

The ordinary differential equation (ODE) system for the moment vector found from the PBE then has the form

$$\frac{dM_k}{dt} = \int_{\mathbb{B}} \xi^k S(t,\xi)\,\mathrm{d}\xi = \overline{S}_k(t) \tag{3}$$

where $\overline{S}_k$ cannot generally be expressed exactly in terms of the moments of f contained in $\mathbf{M}_{2n-1}$. QMOM provides a closure for $\overline{S}_k$ given $\mathbf{M}_{2n-1}$ (McGraw, 1997) of the form

$$\overline{S}_k(t) = \sum_{i=1}^{n} w_i \mathcal{S}_k(t,\xi_i) \tag{4}$$

with non-negative weights $w_i(t)$ and abscissae $\xi_i(t)$. QMOM has the property that if $S(t,\xi) = f(t,\xi)$, then $\mathcal{S}_k(t,\xi_i) = \xi_i^k$ and $\overline{S}_k(t) = M_k(t)$ for $k = 0, 1, \ldots, 2n-1$; meaning that the weights and abscissae corresponds to a Gauss quadrature. Computing these parameters from the moments is a well-known problem solved thanks to the theory of orthogonal polynomials (Gautschi, 2004).

2.2. Monic orthogonal polynomials

Let us recall classical results that can be found in the literature (Dette and Studden, 1997; Gautschi, 2004; Schmüdgen, 2017). For a moment vector $\mathbf{M}_N$, one can define the linear functional $\langle\cdot\rangle$ on the space $\mathbb{R}[X]_N$ of the real polynomial function of degree smaller than N by

$$\langle X^k \rangle = M_k, \quad \text{for } k \in \{0, 1, \ldots, N\}. \tag{5}$$

Then, this linear functional defines a scalar product $(P,Q) \mapsto \langle PQ \rangle$ on $\mathbb{R}[X]_n$, with $n = \lfloor N/2 \rfloor$[1], as soon as $\mathbf{M}_N$ is strictly realizable, i.e., is associated with a positive NDF $f \in L^2(\mathbb{B})$ through eq. (2). In such cases, we have

$$\forall P \in \mathbb{R}[X]_N \qquad \langle P \rangle_{\mathbf{M}_N} = \int_{\mathbb{R}} P(\xi) f(\xi) \mathrm{d}\xi, \tag{6}$$

and we can define a sequence of monic orthogonal polynomials Q_i for $i = 0, \ldots, n$ with Q_i of degree i. This sequence satisfied a three-term recurrence relation:

$$Q_{i+1} = (X - a_i) Q_i - b_i Q_{i-1} \quad \text{for } i = 0, 1, \ldots, n-1 \tag{7}$$

with $Q_0 = 1$ and $Q_{-1} = 0$, and where

$$a_i = \frac{\langle X Q_i^2 \rangle}{\langle Q_i^2 \rangle}, \quad b_i = \frac{\langle Q_i^2 \rangle}{\langle Q_{i-1}^2 \rangle}. \tag{8}$$

Note that a_{n-1} depends on moments up to M_{2n-1} and b_{n-1} up to M_{2n-2}.

Given the moment vector $\mathbf{M}_{2n-1}$, the Chebyshev algorithm (Gautschi, 2004; Wheeler, 1974) finds recurrence coefficients a_i and b_i for $i = 0, 1, \ldots, n-1$. However, it is important to note that adding an even-order moment to get $\mathbf{M}_{2n}$ allows computation of b_n, while adding an odd-order moment to get $\mathbf{M}_{2n+1}$ allows computation of a_n, etc.. This relation is one-to-one, thus the inverse is also true (i.e., the moments can be found from the recurrence coefficients using the reverse Chebyshev algorithm (Fox and Laurent, 2022)). These fundamental properties of orthogonal polynomials are used to define GQMOM in section 3. Although not needed in the following, it is interesting to observe that isomomental distributions (i.e., identical integral moments (McGraw et al., 1998)) will generate the same family of monic orthogonal polynomials.

2.3. Strict realizability characterization

The strict realizability of $\mathbf{M}_N$ is equivalent to the positiveness of certain Hankel determinants (Dette and Studden, 1997; Gautschi, 2004; Schmüdgen, 2017). Thus, let us define these determinants for $d = 0, 1$ and any non-negative k such that $2k + d \leq N$:

$$\underline{H}_{2k+d} = \begin{vmatrix} M_d & M_{1+d} & \ldots & M_{k+d} \\ M_{1+d} & M_{2+d} & \ldots & M_{k+1+d} \\ \vdots & \vdots & \ddots & \vdots \\ M_{k+d} & M_{k+1+d} & \ldots & M_{2k+d} \end{vmatrix}, \tag{9}$$

and

$$\overline{H}_{2k+d} = \begin{vmatrix} M_{1-d} - M_{2-d} & M_{2-d} - M_{3-d} & \ldots & M_k - M_{k+1} \\ M_{2-d} - M_{3-d} & M_{3-d} - M_{4-d} & \ldots & M_{k+1} - M_{k+2} \\ \vdots & \vdots & \ddots & \vdots \\ M_k - M_{k+1} & M_{k+1} - M_{k+2} & \ldots & M_{2k+d-1} - M_{2k+d} \end{vmatrix}. \tag{10}$$

The characterization of the strict realizability of $\mathbf{M}_N$, depending on the choice of $\mathbb{B}$, is as follows:

- If $\mathbb{B} = \mathbb{R}$: $\underline{H}_{2k} > 0$ for $k = 0, \ldots, \lfloor \frac{N}{2} \rfloor$.
- If $\mathbb{B} = \mathbb{R}^+$: $\underline{H}_k > 0$ for $k = 0, \ldots, N$.
- If $\mathbb{B} = (0,1)$: $\underline{H}_k > 0$ and $\overline{H}_k > 0$ for $k = 0, \ldots, N$.

[1] $\lfloor r \rfloor$ is the largest integer less than or equal to the real number r

On the boundary of moment space (i.e., for weakly realizable moments), one (or more) of the Hankel determinants is null. Note that setting a Hankel determinant equal to zero sets the upper/lower bound on its highest-order integral moment.

An equivalent characterization can be done using the coefficients of the three-term recurrence relation of the orthogonal polynomials:

- If $\mathbb{B} = \mathbb{R}$: $b_i > 0$ for $i = 1, \ldots, \lfloor \frac{N}{2} \rfloor$.
- If $\mathbb{B} = \mathbb{R}^+$: existence of $\zeta_i > 0$ for $i = 1, \ldots, N$ such that

$$\begin{cases} a_0 = \zeta_1, & a_i = \zeta_{2i} + \zeta_{2i+1} \quad i = 1, \ldots, \left\lfloor \frac{N-1}{2} \right\rfloor \\ b_i = \zeta_{2i-1}\zeta_{2i} & i = 1, \ldots, \left\lfloor \frac{N}{2} \right\rfloor \end{cases} \tag{11}$$

- If $\mathbb{B} = (0, 1)$: existence of $\zeta_i > 0$ for $i = 1, \ldots, N$ satisfying eq. (11) and existence of $p_i \in (0, 1)$ such that

$$\zeta_1 = p_1, \qquad \zeta_i = p_i(1 - p_{i-1}) \quad i = 2, \ldots, N. \tag{12}$$

Moreover, in the last case, the p_i are referred to as the canonical moments (Dette and Studden, 1997).

Hereinafter, we assume that the known moment vector $\mathbf{M}_{2n}$ is strictly realizable. In any case, this assumption can be verified by applying the Chebyshev algorithm, which computes the recurrence coefficients a_i and b_i from the known moments.

2.4. Moment space and realizability

The moment vector $\mathbf{M}_{2n}$ lies in a convex subset of a linear vector space of dimension $2n + 1$ (Dette and Studden, 1997; Schmüdgen, 2017). We refer to this convex subset as *moment space*. The strict realizability conditions discussed above define the *boundary of moment space*. If $\mathbf{M}_{2n}$ lies in the *interior of moment space*, then it is strictly realizable (all Hankel matrices are positive). A point on the boundary of moment space has at least one of the Hankel matrices equal to zero. Hereinafter, we will use this terminology when describing the properties of various moment closures.

2.5. QMOM closure

The weights w_i and abscissae ξ_i of the Gauss quadrature are found using the recurrence coefficients. (More details on this step are provided in section 3.) Then, the QMOM closure corresponds to replacing $f(\xi)\,\mathrm{d}\xi$ by the finite positive measure $\sum_{i=1}^{n} w_i \delta_{\xi_i}(\xi)$. Thus $M_{2n} = \sum_{i=1}^{n} w_i \xi_i^{2n}$, which is computed by the quadrature, corresponds to $b_n = 0$. This is also the lower bound of all possible M_{2n} such that $\mathbf{M}_{2n}$ is realizable. In contrast, for the truncated Hamburger moment problem (Hamburger, 1944) (i.e. for $\mathbb{B} = \mathbb{R}$) from a strictly realizable moment vector $\mathbf{M}_{2n}$, the odd-order moment M_{2n+1} can take on any finite real value for $\mathbf{M}_{2n+1}$ being realizable. On the other hand, for $\mathbb{B} = \mathbb{R}^+$ and $\mathbb{B} = (0, 1)$ the odd-order moments are also bounded by the realizability constraints.

3. GQMOM for moment vector $\mathbf{M}_{2n}$

The basic idea behind GQMOM is to retain the properties of QMOM while using $N > n \geq 1$ quadrature points found from $\mathbf{M}_{2n}$ with the Chebyshev algorithm. The two principal desired properties are that the source-term closure has the form

$$\overline{S}_k(t) = \sum_{i=1}^{N} w_i \mathcal{S}_k(t, \xi_i), \tag{13}$$

and the moment constraints for $k = 0, 1, \ldots, 2n$ are

$$M_k = \sum_{i=1}^{N} w_i \xi_i^k; \tag{14}$$

i.e., the same as with QMOM but with n replaced by $N \geq n \geq 1$. Roughly speaking, this can be accomplished by choosing realizable moments M_k for $k = 2n+1, 2n+2, \ldots, 2N-1$, and applying the Chebyshev algorithm to $\mathbf{M}_{2N-1}$. This is equivalent to selecting recurrence coefficients a_i for $i = n, n+1, \ldots, N-1$; and $b_i > 0$ for $i = n+1, \ldots, N-1$ that satisfy the realizability constraints in section 2.3. It is important to recall that if the recurrence coefficients are realizable, then we are guaranteed that the quadrature nodes lie in $\mathbb{B}$, and their weights are positive. Expressed in terms of the monic orthogonal polynomials $Q_i(x)$, this selection is done as follows.

3.1. Definition of GQMOM using recurrence coefficients

With GQMOM, the abscissae correspond to the roots of the monic orthogonal polynomial Q_N with $N > n \geq 1$. Thus, we must define the unknown recurrence coefficients (a_i, b_i) for $i = n, n+1, \ldots, N$. First, we start by defining the monic orthogonal polynomials.

3.1.1. Monic orthogonal polynomials

For $i \geq n \geq 1$, we extend the monic orthogonal polynomials in eq. (7) using

$$Q_{i+1} = (x - a_i^{[\mathbf{M}_{2n}]})Q_i - b_i^{[\mathbf{M}_{2n}]}Q_{i-1} \tag{15}$$

where the unknown recurrence coefficients depend on $\mathbf{M}_{2n}$ and are formally defined by eq. (8). For example, $b_n^{[\mathbf{M}_{2n}]} = b_n$ is known, while $a_n^{[\mathbf{M}_{2n}]}$ depends on the closure for $\overline{M}_{2n+1}$ (or vice versa). Hereinafter, an overline is used to denote a closure for a higher-order moment given $\mathbf{M}_{2n}$. In general, the choice for $b_i^{[\mathbf{M}_{2n}]}$ with $i > n$ closes the moment $\overline{M}_{2i}$. As long as $b_i^{[\mathbf{M}_{2n}]} > 0$, this closure will be realizable for $\mathbb{B} = \mathbb{R}$ (Hamburger, 1944), and similar constraints apply for $\mathbb{B} = \mathbb{R}^+$ and $\mathbb{B} = (0, 1)$.

The unknown weight function is $\mu^{[\mathbf{M}_{2n}]} > 0$, i.e., a distribution function on $\mathbb{B}$ with known moments

$$M_k = \int_{\mathbb{B}} \xi^k \, \mathrm{d}\mu^{[\mathbf{M}_{2n}]} \quad \text{for } k = 0, 1, \ldots, 2n; \tag{16}$$

and higher-order moments that depend on $\mathbf{M}_{2n}$:

$$\overline{M}_{2n+k} = \int_{\mathbb{B}} \xi^{2n+k} \, \mathrm{d}\mu^{[\mathbf{M}_{2n}]} \quad \text{for } k \geq 1. \tag{17}$$

The polynomials Q_i are orthogonal:

$$\int_{\mathbb{B}} Q_i Q_j \, \mathrm{d}\mu^{[\mathbf{M}_{2n}]} \, \mathrm{d}\xi = \langle Q_i Q_j \rangle = \gamma_i^{[\mathbf{M}_{2n}]} \delta_{i,j} \tag{18}$$

where

$$\gamma_i^{[\mathbf{M}_{2n}]} = \frac{H_{2i}}{H_{2i-2}} \geq 0 \tag{19}$$

depends on moments up to M_{2i} through the Hankel determinant $H_{2i} = \underline{H}_{2i}$. If, for some k, $\gamma_k^{[\mathbf{M}_{2n}]} = 0$, then $b_m = 0$ for $m \geq k$. This occurs when the Hankel determinant $H_{2k} = 0$ and the moments $\mathbf{M}_{2n}$ are on the boundary of moment space. For clarity, unless stated otherwise, we assume that $\gamma_k^{[\mathbf{M}_{2n}]} > 0$, and thus that $\mathbf{M}_{2n}$ is in the interior of moment space for $\mathbb{B} = \mathbb{R}$. More generally, the GQMOM closure will depend on the definition of the NDF, in particular on $\mathbb{B}$.

3.1.2. Recurrence coefficients for $\mathbb{B} = \mathbb{R}$

In general, choosing the definitions of $a_i^{[\mathbf{M}_{2n}]}$ and $b_i^{[\mathbf{M}_{2n}]}$ for $i > n \geq 1$ corresponds to selecting a form for $\mu^{[\mathbf{M}_{2n}]}$ (among the infinite number of possible choices). Only when $b_n = 0$ is the choice of $\mu^{[\mathbf{M}_{2n}]}$ unique because then $\mathbf{M}_{2n}$ resides on the boundary of moment space. When this is the case, $b_i^{[\mathbf{M}_{2n}]} = 0$ for $i > n$. For

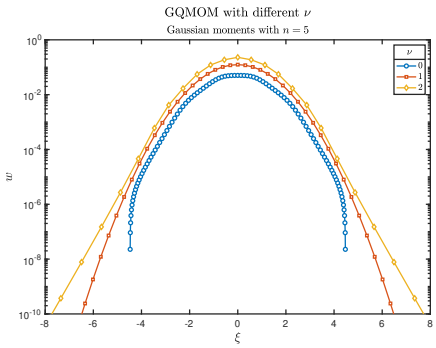

Figure 1: GQMOM quadrature weights versus abscissae for standardized Gaussian moments with $n = 5$, $N = 101$, and different values of ν.

this reason, expressing $b_i^{[\mathbf{M}_{2n}]}$ as proportional to b_n ensures the correct limiting behavior at the boundary of moment space. Moreover, it may be desirable to capture a specific NDF, such as the Gaussian distribution. The recurrence coefficients for the Hermite polynomials, corresponding to a Gaussian distribution, with mean μ and variance σ^2 are

$$a_i^H = \mu, \quad b_i^H = i\sigma^2. \tag{20}$$

These observations lead to the following definition.

Definition 1 (GQMOM with moments $\mathbf{M}_{2n}$ for $n \geq 1$ from a NDF defined on $\mathbb{R}$). *The unknown recurrence coefficients are selected as follows. For $i = n$ in eq. (15), let*

$$a_n^{[\mathbf{M}_{2n}]} = \frac{1}{n}\sum_{i=0}^{n-1} a_i, \quad b_n^{[\mathbf{M}_{2n}]} = b_n. \tag{21}$$

For $i > n$, let

$$a_i^{[\mathbf{M}_{2n}]} = \frac{1}{i}\sum_{k=0}^{i-1} a_k = \frac{1}{n}\sum_{k=0}^{n-1} a_k = a_n^{[\mathbf{M}_{2n}]}, \quad b_i^{[\mathbf{M}_{2n}]} = \left(\frac{i}{n}\right)^{\nu} b_n \tag{22}$$

where the parameter $\nu \in \mathbb{R}$ controls the tails of the distribution function.

The choice for $a_i^{[\mathbf{M}_{2n}]}$ is consistent because it uses the arithmetic average of the known lower-order coefficients. The choice for $b_i^{[\mathbf{M}_{2n}]}$ is based on recovering Gaussian statistics when the known moments $\mathbf{M}_{2n}$ are Gaussian and $\nu = 1$ (i.e., Hermite polynomials). In fig. 1, the weights are shown for different values of ν. Setting $\nu = 2$ gives exponential tails, while $\nu = 0$ gives tails that decay very quickly in a bounded interval.[2] Negative ν forces b_i towards zero (i.e., the boundary of moment space), and eventually multiple modes are observed. The NDF from EM for the first three moments (i.e., $n = 1$) corresponds to $\nu = 1$. Thus, we will refer to the choice $\nu = 1$ as Gaussian–GQMOM. Otherwise, Definition 1 provides a family of GQMOM closures parameterized by ν for moment vectors defined on $\mathbb{R}$.

[2] $\nu = 0$ corresponds to Chebychev polynomials of the second kind for the distribution $\sqrt{1 - (\xi/\xi_{max})^2}$ on the finite interval $(-\xi_{max}, \xi_{max})$ with $\xi_{max} = 2\sqrt{b_1}$, which are the special case of the shifted Jacobi polynomials with $\alpha = \beta = 1/2$.

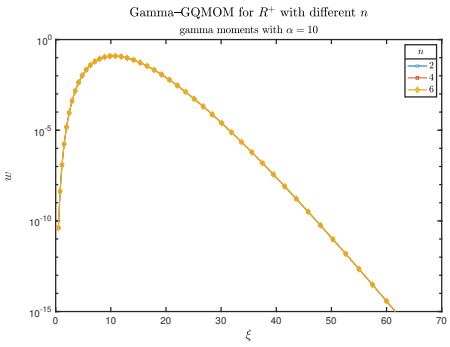

Figure 2: Gamma–GQMOM quadrature weights versus abscissae for gamma moments with $\alpha = 10$, $N = 101$, and different values of n.

3.1.3. Recurrence coefficients for $\mathbb{B} = \mathbb{R}^+$

Due to the additional constraint of $\underline{H}_{2n+1} > 0$, different choices for $a_i^{[\mathbf{M}_{2n}]}$ and $b_i^{[\mathbf{M}_{2n}]}$ are needed for strictly positive variables. In this case, it is convenient to introduce the sequence of positive ζ_i with $a_0 = \zeta_1$ and

$$a_i = \zeta_{2i} + \zeta_{2i+1}, \quad b_i = \zeta_{2i-1}\zeta_{2i}. \tag{23}$$

Thus, selecting $\zeta_i^{[\mathbf{M}_{2n}]}$ for $i > 2n$ is equivalent to choosing $a_i^{[\mathbf{M}_{2n}]}$ and $b_i^{[\mathbf{M}_{2n}]}$. The Chebyshev algorithm computes a_i and b_i from the moments $\mathbf{M}_{2n}$, and then eq. (23) is inverted to find ζ_i for $1 \leq i \leq 2n$. For the GQMOM closure, we can select the additional ζ_i to produce the generalized Laguerre polynomials for moments from a gamma NDF where $f(x) \propto x^\alpha e^{-\beta x}$ and $\beta > 0$. The ζ_i in this case are, for $i \geq 1$:

$$\zeta_{2i-1}^L = \frac{i+\alpha}{\beta}, \qquad \zeta_{2i}^L = \frac{i}{\beta}. \tag{24}$$

Note that β is a scaling parameter, while α changes the shape of the NDF and is dimensionless. These two parameters are fixed given the mean and variance of the NDF. These properties lead to the following definition.

Definition 2 (Gamma–GQMOM with moments $\mathbf{M}_{2n}$ for $n \geq 1$ from a NDF defined on $\mathbb{R}^+$). *Let*

$$\alpha = \frac{M_1^2}{M_2 M_0 - M_1^2} - 1.$$

Then $\alpha > -1$ and the unknown recurrence coefficients are selected as follows. For $i > n \geq 1$, let

$$\zeta_{2i-1}^{[\mathbf{M}_{2n}]} = \frac{i+\alpha}{n+\alpha}\zeta_{2n-1}, \quad \zeta_{2i}^{[\mathbf{M}_{2n}]} = \frac{i}{n}\zeta_{2n}. \tag{25}$$

Thus, for $i > n \geq 1$, in eq. (15) the recurrence coefficients are

$$a_i^{[\mathbf{M}_{2n}]} = \zeta_{2i}^{[\mathbf{M}_{2n}]} + \zeta_{2i+1}^{[\mathbf{M}_{2n}]}, \quad b_i^{[\mathbf{M}_{2n}]} = \zeta_{2i-1}^{[\mathbf{M}_{2n}]}\zeta_{2i}^{[\mathbf{M}_{2n}]}. \tag{26}$$

In fig. 2, the weights and abscissae are shown for gamma–PDF moments with $\alpha = 10$ and $\beta = 1$ and three different values of n. In all cases, the abscissas are positive and do not depend on n. The NDF from EM with the same zero- and first-order moments corresponds to $\alpha = 0$ (i.e., an exponential NDF).

Another possibility is to select the additional ζ_i to produce the Stieltjes–Wigert polynomials for moments from a lognormal NDF:

$$f(\xi) \propto \frac{1}{\xi\sigma\sqrt{2\pi}} \exp\left(-\frac{(\ln(\xi)-\mu)^2}{2\sigma^2}\right). \tag{27}$$

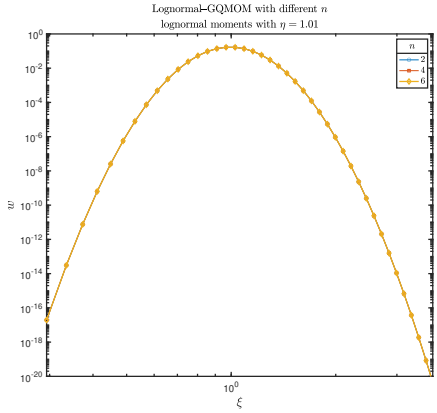

Figure 3: Lognormal–GQMOM quadrature weights versus abscissae for lognormal moments with $\eta = 1.01$, $N = 201$, and different values of n.

The ζ_i in this case are, for $i \geq 1$, denoting $\eta = \exp(\sigma^2/2) > 1$ (Madadi-Kandjani and Passalacqua, 2015; Wilck, 2001):

$$\zeta^W_{2i-1} = e^{\mu}\eta^{4i-3}, \qquad \zeta^W_{2i} = e^{\mu}\eta^{2i-1}(\eta^{2i} - 1). \tag{28}$$

These properties lead to the following definition.

Definition 3 (Lognormal–GQMOM with moments $\mathbf{M}_{2n}$ for $n \geq 1$ from a NDF defined on $\mathbb{R}^+$). *Let*

$$\eta = \sqrt{\frac{M_2 M_0}{M_1^2}}. \tag{29}$$

With $\eta > 1$, the recurrence coefficients for $i > n \geq 1$ are found from eq. (26) using

$$\zeta^{[\mathbf{M}_{2n}]}_{2i-1} = \eta^{4(i-n)}\zeta_{2n-1}, \quad \zeta^{[\mathbf{M}_{2n}]}_{2i} = \eta^{2(i-n)}\left(\frac{\eta^{2i}-1}{\eta^{2n}-1}\right)\zeta_{2n}. \tag{30}$$

In fig. 3, the weights and abscissae are shown for three different values of n with lognormal moments and $\eta = 1.01$. Again, the abscissae are positive and do not depend on n, but many have weights below 10^{-15} due to the long tail of the lognormal NDF.

3.1.4. Recurrence coefficients for $\mathbb{B} = (0, 1)$

For the finite interval $(0, 1)$, we define GQMOM using the canonical moments $p_i \in (0, 1)$, which are related to the ζ_i by

$$\zeta_i = p_i(1 - p_{i-1}) \tag{31}$$

for $1 \leq i \leq 2n$ with $p_0 = 0$. For this purpose, the Chebyshev algorithm with input $\mathbf{M}_{2n}$ can be easily modified to compute the p_i from the ζ_i found from eq. (23). Here, the choice for p_i produces the Jacobi polynomials for moments from a beta NDF where $f(x) \propto x^{\beta}(1 - x)^{\alpha}$, but also that the quadrature nodes are always in the interval $(0, 1)$, which is the condition for the strict realizability. The canonical moments in this case are, for $i \geq 1$:

$$p^J_{2i-1} = \frac{\beta + i}{2i + \alpha + \beta}, \qquad p^J_{2i} = \frac{i}{2i + 1 + \alpha + \beta}. \tag{32}$$

The two parameters α and β are fixed given the mean and variance of the NDF. These properties lead to the following definition.

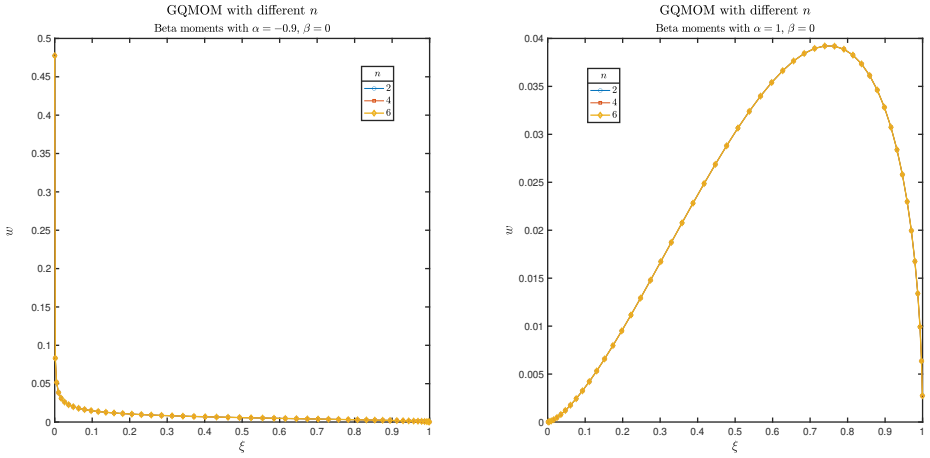

Figure 4: Beta–GQMOM quadrature weights versus abscissae for beta-NDF moments in $(0, 1)$ with $N = 51$ and different values of n.

Definition 4 (Beta–GQMOM with moments $\mathbf{M}_{2n}$ for $n \geq 1$ from a NDF defined on $(0, 1)$). *The unknown recurrence coefficients are selected as follows. Let*

$$\alpha = \frac{1 - p_1 - 2p_2 + p_1 p_2}{p_2}, \quad \beta = \frac{p_1 - p_2 - p_1 p_2}{p_2} \tag{33}$$

and, for $i > n \geq 1$,

$$p_{2i-1}^{[\mathbf{M}_{2n}]} = \begin{cases} p_{2n-1} \frac{p_{2i-1}^J}{p_{2n-1}^J} & \text{if } p_{2n-1} \leq p_{2n-1}^J \text{ or } p_{2n-1}^J \geq p_{2i-1}^J, \\ \frac{p_{2n-1}(1-p_{2i-1}^J)+p_{2i-1}^J-p_{2n-1}^J}{1-p_{2n-1}^J} & \text{otherwise.} \end{cases} \tag{34}$$

$$p_{2i}^{[\mathbf{M}_{2n}]} = \begin{cases} p_{2n} \frac{p_{2i}^J}{p_{2n}^J} & \text{if } p_{2n} \leq p_{2n}^J \text{ or } p_{2n}^J \geq p_{2i}^J, \\ \frac{p_{2n}(1-p_{2i}^J)+p_{2i}^J-p_{2n}^J}{1-p_{2n}^J} & \text{otherwise.} \end{cases} \tag{35}$$

These provide $\zeta_i^{[\mathbf{M}_{2n}]} = p_i^{[\mathbf{M}_{2n}]}(1 - p_{i-1}^{[\mathbf{M}_{2n}]})$ for $i > 2n$, and hence, with eq. (26), $a_i^{[\mathbf{M}_{2n}]}$ and $b_i^{[\mathbf{M}_{2n}]}$ for $i > n$.

In fig. 4, the weights and abscissae are shown for moments from a beta NDF for different values of $\alpha, \beta > -1$. As can be observed, the abscissas remain bounded in $(0, 1)$ and the quadrature points are the same for all n. By a linear change of variables, beta–GQMOM on $(0, 1)$ can be shifted to define a Gauss quadrature for any finite interval (a, b).

3.2. Generalized QMOM for $\mathbf{M}_{2n-1}$

When working with a legacy code based on QMOM, it may be convenient to use $\mathbf{M}_{2n-1}$ instead of $\mathbf{M}_{2n}$ for $n \geq 1$. Because $\mathbf{M}_{2n-1}$ contains moments only up to order $2n - 1$ (and not $2n$), b_n is unknown. However, for example, we can still use the procedure in eq. (22) to define b_n given b_{n-1}. Thus, a sequence of orthogonal polynomials can also be defined for this case. These polynomials can then be used to close even-order moments starting at order $2n$. For example, for $n = 2$ with $\mathbf{M}_3 = (1, 0, 1, S_3)$ and Gaussian–GQMOM, we find $b_2 = 2$ and hence the standardized fourth-order moment is $3 + S_3^2$. As before, the closed moments will be in the interior of moment space as long as $b_{n-1} > 0$. In summary, GQMOM can be used with either $\mathbf{M}_{2n-1}$ or $\mathbf{M}_{2n}$. However, for consistency with EQMOM (Yuan et al., 2012), unless stated otherwise, hereinafter we will use $\mathbf{M}_{2n}$.

3.3. Computation of weights and abscissas with GQMOM

As done with QMOM (McGraw, 1997; Wheeler, 1974), the N weights and N abscissae are found from the eigenvectors and eigenvalues, respectively, of the following Jacobi matrix:

$$\mathbf{J}_N = \begin{pmatrix} a_0 & \sqrt{b_1} & & & \\ \sqrt{b_1} & a_1 & \sqrt{b_2} & & \\ & \ddots & \ddots & \ddots & \\ & & \sqrt{b_{N-2}} & a_{N-2} & \sqrt{b_{N-1}} \\ & & & \sqrt{b_{N-1}} & a_{N-1} \end{pmatrix}. \tag{36}$$

Using the definitions in eq. (21) and eq. (22), it is straightforward to modify the Chebyshev algorithm in Fox and Laurent (2022) to construct $\mathbf{J}_N$ given the moments $\mathbf{M}_{2n}$, and then to find the weights and abscissae.

By construction, the GQMOM quadrature satisfies eq. (14). The source terms in the moment equations eq. (3) are closed using eq. (13). Unlike with QMOM, with GQMOM the value of N can be very large as long as n is not too large ($n \leq 10$). Notwithstanding, increasing N with fixed n does not increase our knowledge of the unknown NDF governed by the PBE. Thus, as with the secondary quadrature in EQMOM (Yuan et al., 2012), increasing N is only needed to reduce the quadrature error on $\overline{S}_k$. In other words, for fixed n, the value of N can be increased until $\overline{S}_k$ satisfies a convergence criterion for all k. Source code for GQMOM is available at `https://openqbmm.org/`.

4. Numerical examples and validation

In this section we provide numerical examples for problems that are difficult to treat using QMOM. First, to illustrate the differences between QMOM and GQMOM, we show examples of NDF composed of three modes. Recall that with $n = 1$, GQMOM corresponds to a known NDF (e.g., Gaussian) while for QMOM, it corresponds to a Dirac delta function. By increasing n, it is possible to approximate a multi-modal NDF. It is important to understand that QMOM with $\mathbf{M}_{2n-1}$ represents the NDF by the sum of n Dirac delta functions, and, given the additional moment M_{2n}, GQMOM provides a continuous NDF. Heuristically, for fixed $\mathbf{M}_{2n-1}$ GQMOM spreads out the n Dirac delta functions found with QMOM as M_{2n} increases from its minimum value. Thus, with sufficiently large M_{2n}, the GQMOM NDF will become mono-modal, losing all resemblance with the QMOM NDF.

Generally speaking, if the time evolution of the moments of a NDF are adequately captured with QMOM, then GQMOM will provide equivalent accuracy. Thus, in the numerical examples starting in section 4.2, we focus on systems for which QMOM is known to have difficulties. While such systems are relatively rare in real applications, we shall see that GQMOM offers a viable alternative to QMOM for such cases.

4.1. Trimodal Gaussian

Recalling that the objective of GQMOM is to provide a more accurate N-node quadrature for fixed n, we compute the moments to arbitrary order from a trimodal Gaussian NDF composed of three Gaussian NDF with different means and standard deviations. Using QMOM, such a distribution requires at least $n = 3$ to capture the locations of the three modes, and $n \geq 6$ to capture their variances. Here, we take the weights of the three Gaussian NDF to be equal, their means to be $(-3, 0, 4)$ with standard deviations, respectively, of $(1/10, 1/20, 1/30)$. The quadratures found with Gaussian–GQMOM ($N = 101$) and QMOM are shown in fig. 5 for $n = 3, 6, 9$. The GQMOM result with $n = 3$ consists of two delta functions at approximately $\xi = -3$ and 4, and a Gaussian distribution centered at $\xi = 0$ with significant variance. As n increases, the weights take values that more closely correspond to the true NDF. Consistent with EQMOM, we observe that the value of n mainly determines the quality of the reconstruction, while N provides "extra" refinement. The latter is needed to converge the source-term closure in eq. (13) for a given n.

In most cases, $N = 3n$ provides adequate refinement, but larger N may be needed for highly nonlinear, localized, source terms. This point is illustrated in fig. 6 using a trimodal NDF on $(0, 1)$ with beta–GQMOM. In this figure, the weights are scaled to sum to N and $n = 6$ is held constant. With $N = 6$, the mean and

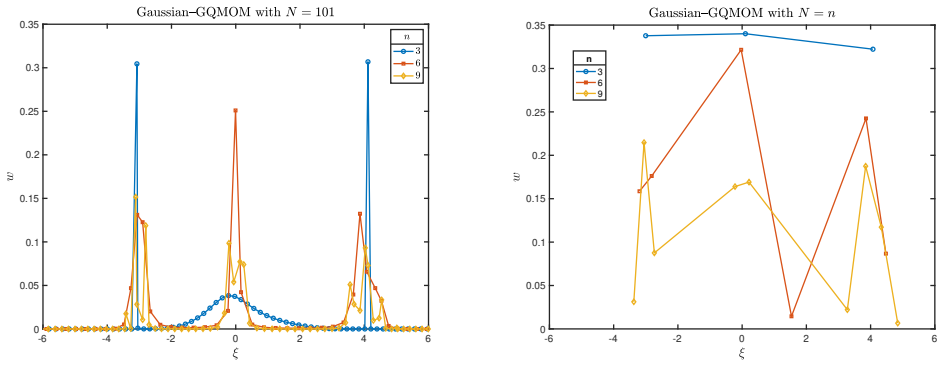

Figure 5: Trimodal Gaussian NDF on $\mathbb{R}$ with $n = 3, 6, 9$. Left: Gaussian-GQMOM with $N = 101$. Right: QMOM. The quadrature points are connected by lines to ease interpretation.

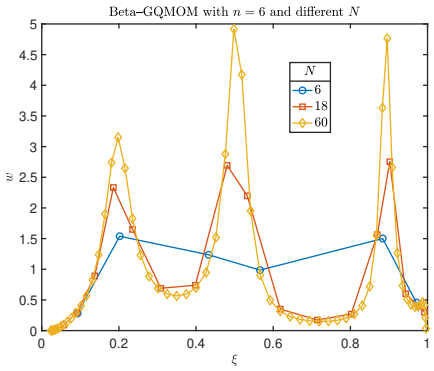

Figure 6: Trimodal NDF on $(0, 1)$ with $n = 6$ and different N. Weights are scaled to sum to N.

variance of each mode is roughly captured. Increasing to $N = 3n = 18$ provides several more quadrature points for each peak, while $N = 60$ covers the full domain with roughly equal-spaced points. In all cases, because GQMOM reproduces the same moments as QMOM, using $N > n$ does not produce a poorer quality quadrature for fixed n. In practice, a NDF with up to five modes can be approximated with GQMOM to reasonable accuracy.

4.2. Application to aggregation and breakup problems

We consider in this section an application of GQMOM to a PBE involving aggregation and breakup. Cases 5 and 8 studied in prior work (Madadi-Kandjani and Passalacqua, 2015; Vanni, 2000) are examined here, since they allow for a direct comparison of the results obtained with GQMOM to those provided by EQMOM in Madadi-Kandjani and Passalacqua (2015), and to the exact solution found in Vanni (2000). For all other cases in Madadi-Kandjani and Passalacqua (2015), QMOM yields an accurate solution without the additional quadrature nodes provided by GQMOM. For consistency, we maintain the same case numbers used in Madadi-Kandjani and Passalacqua (2015).

The 1-D NDF describing the particle size ξ is $f(t, \xi)$, and its temporal evolution is regulated by the following PBE:

$$\frac{\partial f(t,\xi)}{\partial t} = \bar{B}^a(t,\xi) - \bar{D}^a(t,\xi) + \bar{B}^b(t,\xi) - \bar{D}^b(t,\xi). \tag{37}$$

Following Marchisio and Fox (2013); Marchisio et al. (2003); Randolph and Larson (1988), the source terms

for aggregation and breakage are expressed as

$$\bar{B}^a(t,\xi) = \frac{\xi^2}{2}\int_0^{\xi} \frac{\beta((\xi^3-\xi'^3)^{1/3},\xi')}{(\xi^3-\xi'^3)^{2/3}} f(t,(\xi^3-\xi'^3)^{1/3}) f(t,\xi')\,\mathrm{d}\xi', \tag{38}$$

$$\bar{D}^a(t,\xi) = f(t,\xi)\int_0^{\infty} \beta(\xi,\xi') f(t,\xi')\,\mathrm{d}\xi', \tag{39}$$

$$\bar{B}^b(t,\xi) = \int_{\xi}^{\infty} a(\xi') b(\xi|\xi') f(t,\xi')\,\mathrm{d}\xi', \tag{40}$$

$$\bar{D}^b(t,\xi) = a(\xi) f(t,\xi). \tag{41}$$

The application of eq. (2) to both sides of eq. (37) leads to the evolution equation for the moment M_k of the NDF:

$$\frac{dM_k(t)}{dt} = \bar{B}_k^a(t) - \bar{D}_k^a(t) + \bar{B}_k^b(t) - \bar{D}_k^b(t). \tag{42}$$

For consistency with prior work, in this example we use the moment vector $\mathbf{M}_5$. The source terms for the moments are defined as follows:

$$\begin{aligned}
\bar{B}_k^a(t) &= \frac{1}{2}\int_0^{\infty} f(t,\xi')\int_0^{\infty} \beta(\xi,\xi')(\xi^3+\xi'^3)^{k/3} f(t,\xi)\,\mathrm{d}\xi\,\mathrm{d}\xi',\\
\bar{D}_k^a(t) &= \int_0^{\infty} \xi^k f(t,\xi)\int_0^{\infty} \beta(\xi,\xi') f(t,\xi')\,\mathrm{d}\xi'\,\mathrm{d}\xi,\\
\bar{B}_k^b(t) &= \int_0^{\infty} \xi^k \int_0^{\infty} a(\xi') b(\xi|\xi') f(t,\xi')\,\mathrm{d}\xi'\,\mathrm{d}\xi,\\
\bar{D}_k^b(t) &= \int_0^{\infty} \xi^k a(\xi) f(t,\xi)\,\mathrm{d}\xi.
\end{aligned} \tag{43}$$

The integrals in eq. (43) are approximated as shown in eq. (4), when using GQMOM, by replacing n with N to use all the additional nodes. The EQMOM integration strategy for eq. (42) is summarized in Appendix A, and further details can be found in Madadi-Kandjani and Passalacqua (2015); Yuan et al. (2012). Table 1 summarizes the closure models used in the two test cases considered here, while the daughter distribution functions $b\,(\xi|\xi')$ are listed in table 2.

The time evolution of the volume-average diameter $d_{43} = M_4/M_3$ is reported in fig. 7, where results are shown for gamma–GQMOM, as well as for the lognormal–EQMOM (Madadi-Kandjani and Passalacqua, 2015), and the exact solution (Vanni, 2000). We consider the same cases to investigate the convergence of gamma–GQMOM with the number of nodes, while maintaining the number of QMOM quadrature nodes constant and equal to $n = 3$ (6 moments), and increasing the number N of gamma–GQMOM nodes. We consider $N = 4, 5, 10, 50, 100$ for Case 5 and $N = 4, 5, 10, 50, 100, 150$ for Case 8.

From the time evolution of d_{43} reported in fig. 8, no variation can be visually observed in the solutions obtained with gamma–GQMOM using different N. A more interesting behavior is observed in Case 8, for which the time evolution of d_{43} is shown in fig. 9. In this case, QMOM with $n = 3$ is insufficient to capture the asymptotic behavior. Adding another gamma–GQMOM node for the same moments leads to correctly predict the trend but not the asymptotic value. However, the gamma–GQMOM prediction appears to converge for $N > 50$. Specifically, for the cases run with $N = 100$ and 150 the percentage difference between the asymptotic values of d_{43} is 0.0462%.

Table 1: Cases examined for the aggregation and breakup process using $\mathbf{M}_5$. M_6 is reported in Case 8 for EQMOM.

Case	$\beta(\xi,\xi')$	$a(\xi)$	$b(\xi\|\xi')$	$M_k(t=0)$
5	1	$\begin{cases} 0 & \xi = 1 \\ 0.02 & \xi > 1 \end{cases}$	1, table 2	$M_k = 1, k = 0, \ldots, 5$
8	$(\xi + \xi')^2 \lvert\xi^2 - \xi'^2\rvert$	$\begin{cases} 0 & \xi = 1 \\ 0.01\xi^6 & \xi > 1 \end{cases}$	2, table 2	$\begin{cases} M_0 = 1 \\ M_1 = 1.13 \\ M_2 = 1.294 \\ M_3 = 1.5 \\ M_4 = 1.760 \\ M_5 = 2.087 \\ M_6 = 2.513 \end{cases}$

Table 2: Daughter distribution functions and their moment transforms.

No.	Mechanism	$b(\xi\|\xi')$	$\bar{b}^k(\xi)$
1	Symmetric fragmentation	$\begin{cases} 2 & \xi = \frac{\xi'}{2^{1/3}} \\ 0 & \text{otherwise} \end{cases}$	$2^{(3-k)/3}\xi^k$
2	Uniform	$\begin{cases} \frac{6\xi^2}{\xi'^3} & \xi \in (0,\xi') \\ 0 & \text{otherwise} \end{cases}$	$\frac{6\xi^k}{k+3}$

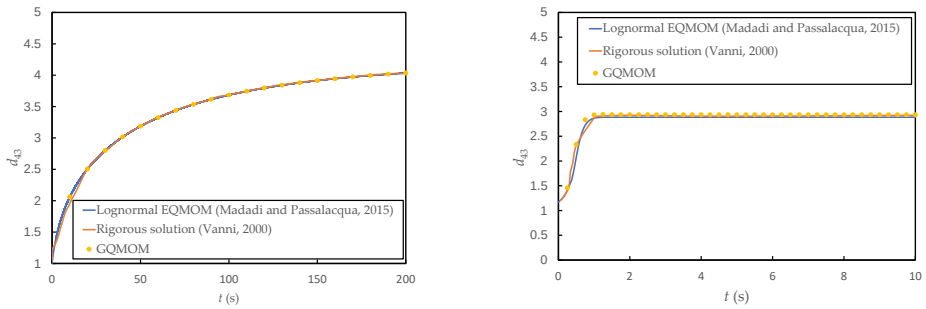

(a) Case 5

(b) Case 8

Figure 7: Time evolution of d_{43} obtained with gamma–GQMOM, lognormal–EQMOM Madadi-Kandjani and Passalacqua (2015), and the exact solution Vanni (2000).

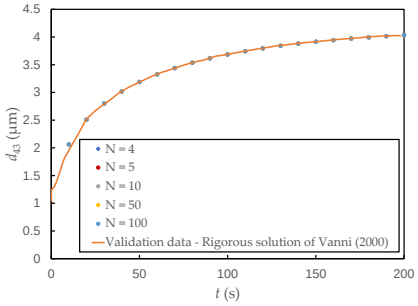

Figure 8: Case 5: Time evolution of d_{43} with increasing N.

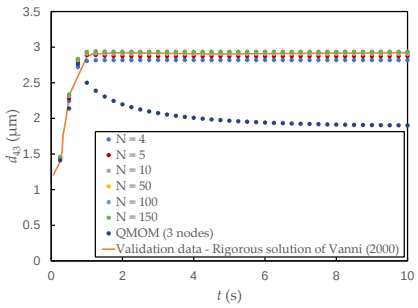

Figure 9: Case 8: Time evolution of d_{43} with $n = 3$ and increasing N.

4.3. Example with a localized source term

In this section, we consider an application of GQMOM to a PBE involving nucleation, growth and filtration, as can occur in suspension crystallization processes (Grosch et al., 2007) or aerosol filtration. Here, the nucleation is assumed to create particles of fixed size ξ_0, at a constant rate φ, the growth rate G is assumed to be constant, and the filtration term describes the removal of particles of size larger than ξ_1. This PBE is used, for example, to model the effect of an ideal fine trap (Grosch et al., 2007). We then consider the following PBE for the NDF $f(t,\xi)$:

$$\frac{\partial f(t,\xi)}{\partial t} = \varphi\delta_{\xi_0}(\xi) - \partial_\xi(Gf(t,\xi)) - \alpha f(t,\xi) I_{[\xi_1,+\infty)}(\xi). \tag{44}$$

where the identity function $I_{[a,+\infty)}(x)$ is zero for $x < a$ and 1 elsewhere. Let us remark that $f\left(t, \frac{\xi-\xi_0}{\xi_1-\xi_0}\right)$ is the solution of a similar PBE with scaled parameters, in such a way that we can choose $\xi_0 = 0$ and $\xi_1 = 1$ without loss of generality. Finally, the values of the parameters used here are $\varphi = 1$, $G = 2$ and $\alpha = 10$, in this non-dimensional context. The main difficulty of this PBE lies in the filtration term, which is localized in phase space so that it only affects particles with size $\xi \geq \xi_1$. Indeed, quadrature-based methods usually give very good results for the growth term (McGraw, 1997), even with a non-constant rate $G(\xi)$, and the nucleation term is already closed in the moment equations.

The analytical solution of eq. (44), with the zero initial condition $f(0,\xi) = 0$, is

$$f(t,\xi) = \frac{\varphi}{G}\begin{cases} 0 & \text{if } \xi < \xi_0 \\ 1 & \text{if } \xi_0 \leq \xi \leq \min(\xi_1, \xi_0 + tG) \\ \exp\left(-\frac{\alpha}{G}(\xi - \xi_1)\right) & \text{if } \xi_1 \leq \xi \leq \xi_0 + tG \end{cases}, \tag{45}$$

so that the moments of the NDF are

$$m_k(t) = \frac{\varphi}{G}\left(\frac{\min(\xi_0 + tG, \xi_1)^{k+1} - \xi_0^{k+1}}{k+1} + \int_0^{\max(0,\xi_0-\xi_1+tG)} (\xi_1 + s)^k \exp\left(-\frac{\alpha}{G}s\right) \mathrm{d}s\right). \tag{46}$$

Using GQMOM with $\mathbf{M}_{2n}$, the equations for the moments are written, for $k = 0, 1, \ldots, 2n$, as

$$\frac{dM_k(t)}{dt} = \varphi\xi_0^k + kGM_{k-1}(t) - \alpha\int_{\xi_1}^{+\infty} \xi^k \,\mathrm{d}\mu^{[\mathbf{M}_{2n}]}. \tag{47}$$

For their resolution, an operator splitting is introduced. During one time step Δt, the growth term is first solved, followed by the resolution of the others terms. Each operator is solved analytically, using the underlying representation of the moments as a sum of Dirac delta functions. Then, for the growth operator, each abscissa of the quadrature is increased by $G\Delta t$. For the nucleation and filtration operators, the weights corresponding to abscissa greater than ξ_1 are multiplied by $\exp(-a\Delta t)$ and $\varphi\xi_0^k\Delta t$ is added to the corresponding moment of order k, for $k = 0\ldots, 2n$. Moreover, a small enough time step (5×10^{-6}) is chosen to ensure time convergence.

The simulations are done using five moments $\mathbf{M}_4$ and $N = 20$ abscissas with gamma–GQMOM and gamma–GQMOM–Radau. Here, Radau quadrature refers to a Gaussian quadrature where one abscissa is fixed (Gautschi and Li, 1991). These results are compared with the analytical solution in fig. 10. As seen from these plots, gamma–GQMOM–Radau seems to be well adapted to this test case: compared to gamma–GQMOM, an abscissa is fixed at $\xi = 0$, which is the nuclei size. And then, gamma–GQMOM–Radau gives better results than gamma–GQMOM, even if gamma–GQMOM also has good results for a larger number of abscissas (not shown here). These methods are also compared to QMOM–Radau, whose results for M_0 are quite good, but the error increases with the order of the moments. Gamma–EQMOM is also tested with ten secondary quadrature points, so that the cost is quite similar to gamma–GQMOM. However, gamma–EQMOM gives the worst results, even if these results can be improved by using a much larger number of secondary quadrature points (not shown here).

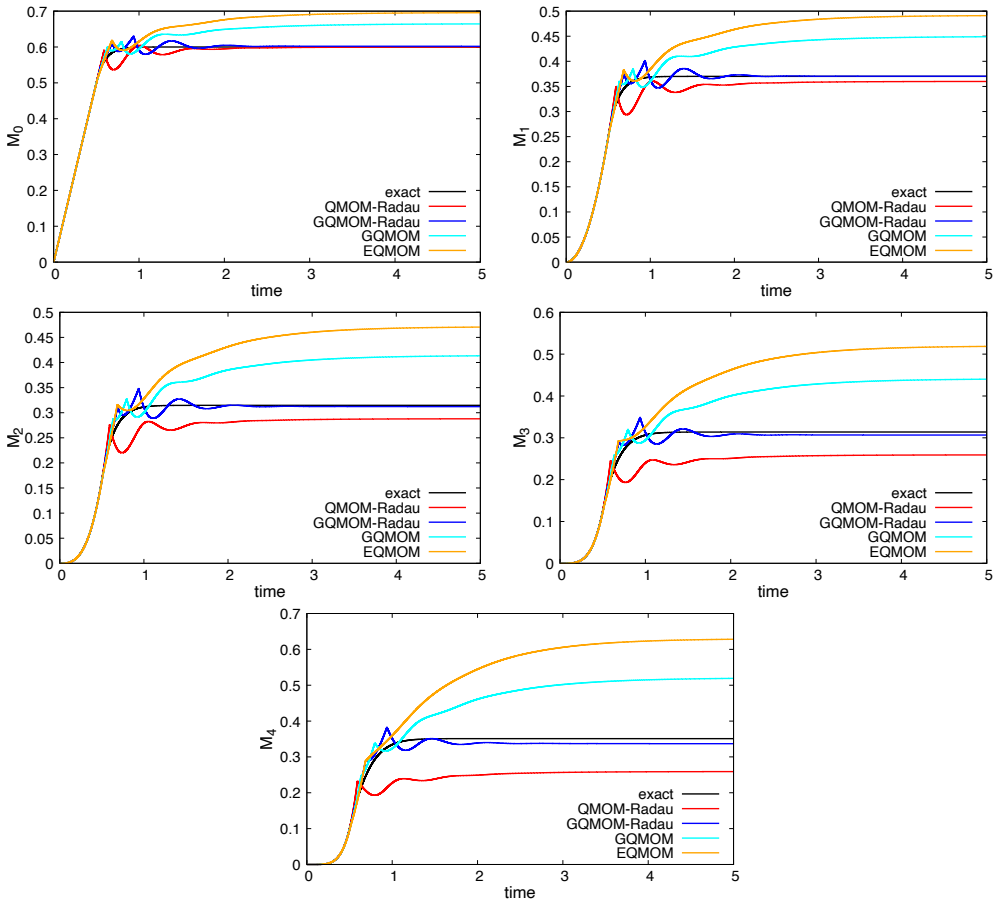

Figure 10: Test case with nucleation, growth and filtration: moments of order 0, 1, 2, 3 and 4 for the analytical solution, QMOM–Radau with five moments (i.e., $\mathbf{M}_4$), gamma–GQMOM and gamma–GQMOM–Radau with five moments and $N = 20$ and gamma–EQMOM with 10 secondary quadrature points.

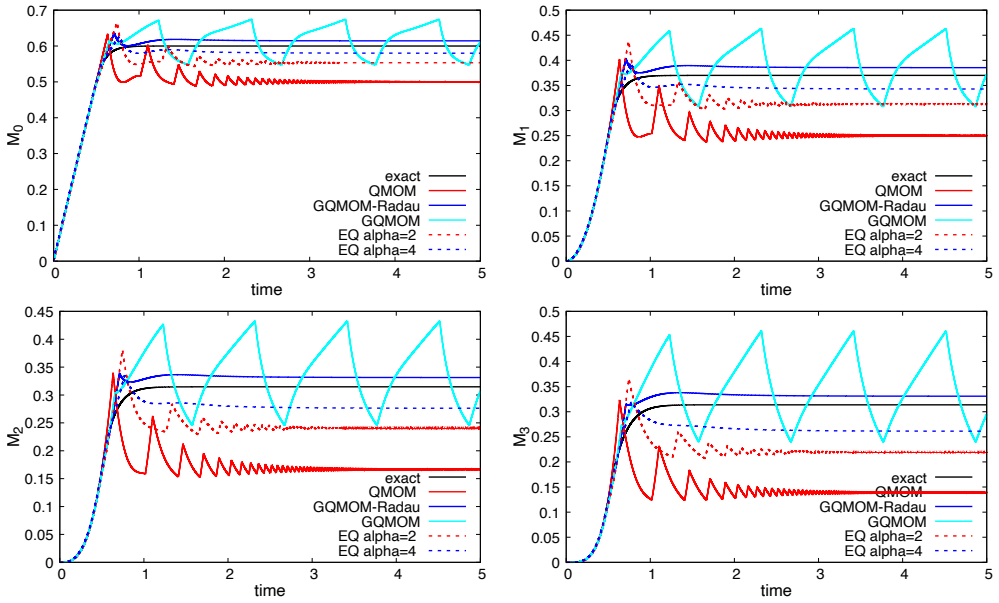

Figure 11: Comparison of different closures for test case with nucleation, growth and filtration: moments of order 0, 1, 2 and 3 for the analytical solution, QMOM with four moments (i.e., $\mathbf{M}_3$), gamma–GQMOM and gamma–GQMOM–Radau with four moments and entropic quadrature (EQ) with multiplicative factor $\alpha = 2$ and $\alpha = 4$.

Finally, to compare GQMOM with another method from the literature, entropic quadrature (EQ) developed by Böhmer and Torrilhon (2020), simulations using four moments $\mathbf{M}_3$ are done. In fig. 11 the results are plotted with gamma–GQMOM and gamma–GQMOM–Radau using $N = 20$ quadrature points, QMOM, and EQ with multiplicative factor $\alpha = 2$ and $\alpha = 4$ and the smallest abscissa fixed at $\xi = 0$. The best results are obtained with gamma–GQMOM–Radau even if the moments are slightly overestimated, whereas the other methods show an oscillatory behavior. In any case, it is very interesting to observe how using Radau quadrature in the presence of nucleation significantly improves the predictions of GQMOM, even with a relatively small number of moments. Also, comparing fig. 11 with fig. 10, we see that using gamma–GQMOM–Radau with $\mathbf{M}_4$ is significantly more accurate than with $\mathbf{M}_3$. This is consistent with observations made with other systems, i.e., moment vectors terminating with an even-order moment usually provide more accurate results.

4.4. Symmetric binary breakup

We consider next the apparently very simple test case of symmetric binary breakup. Depending on the initial conditions, it has been shown that this test case can lead to some difficulties for QMOM, such as convergence to an incorrect solution (Peterson et al., 2022). Thus, let us consider the following PBE for the NDF $f(t, v)$:

$$\partial_t f(t, v) = -g(v) f(t, v) + 4g(2v) f(t, 2v) \tag{48}$$

with the initial condition $f(0, v) = f^0(v)$. Moreover, the simple case $g(v) = v$ suffices to illustrate the difficulties. Using GQMOM with $\mathbf{M}_{2n-1}$, the equations for the moments are written, for $k = 0 \ldots, 2n - 1$, as

$$\frac{dM_k(t)}{dt} = (-1 + 2^{1-k}) M_{k+1}(t). \tag{49}$$

Let us remark that, due to the simple choice for g, only M_{2n} has to be closed. This set of equations is solved using an adaptive time-step algorithm (Nguyen et al., 2016) based on embedded SSP explicit Runge–Kutta

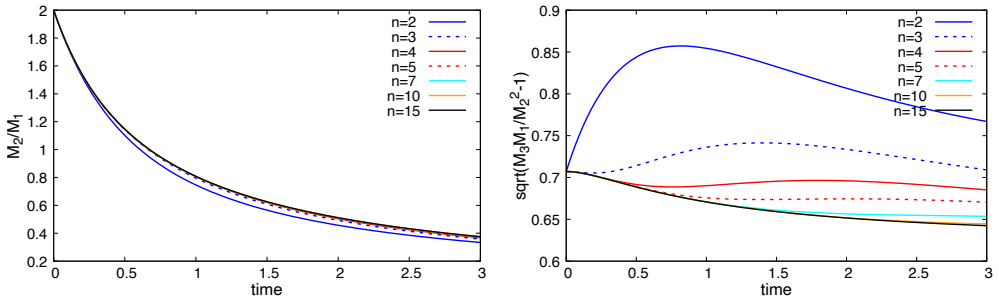

Figure 12: Fragmentation, Case 1: mean (left) and variance (right) obtained for simulations with QMOM with a number of abscissas n equal to 2, 3, 4, 5, 7, 10, 15.

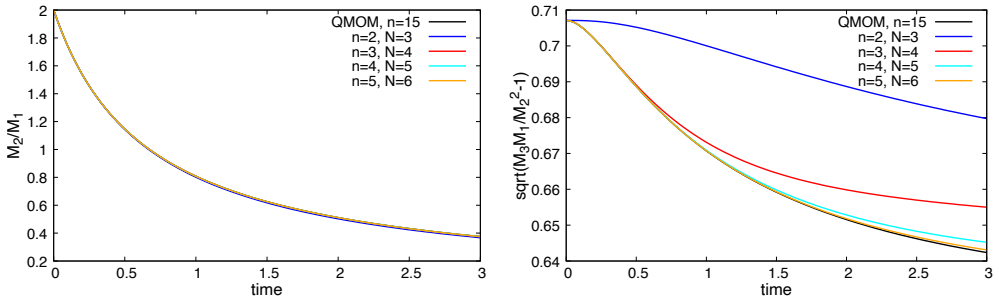

Figure 13: Fragmentation, Case 1: reference solution using QMOM and mean (left) and variance (right) obtained for simulations with gamma–GQMOM with a number of moments $2n$ equal to 4, 6, 8, 10; and a number of quadrature points equal to $n+1$.

methods, with a time-step selection designed both to control the error and to ensure the realizability of the moment set.

For the initial distribution, two cases are considered:

- Case 1: $f^0(v) = \exp(-v)$.
- Case 2: $f^0(v)$ is a lognormal distribution: with $v_0 = 1$, $\sigma_0 = 2$:

$$f^0(v) = \frac{1}{v\sigma\sqrt{2\pi}} \exp\left(-\frac{\ln(v)-\mu}{2\sigma^2}\right), \quad \mu = \ln\left(\frac{v_0}{\sqrt{1+\sigma_0^2}}\right), \quad \sigma^2 = \ln(1+\sigma_0^2).$$

As in Peterson et al. (2022), we look at the mean M_2/M_1 and variance $\sqrt{M_3M_1/M_2^2 - 1}$ of the volume distribution. For Case 1, we can see in fig. 12 that using QMOM, the results converge when the number of moments increases to the value given in Peterson et al. (2022). With gamma–GQMOM, only one additional quadrature point is used compared to QMOM. Due to the simple form of the equations, all simulations with a higher number of quadrature points give the same results. It can be seen in fig. 13 that gamma–GQMOM converges to the same mean value and variance as QMOM, when the number of moments increases, but also faster than QMOM: about half the number of moments are needed for the same accuracy.

Case 2 was shown in Peterson et al. (2022) to be difficult for QMOM, i.e., the method converges to the wrong solution. In fig. 14, we compared the mean value and variance obtained with QMOM, gamma–GQMOM and lognormal–GQMOM, using a large enough number of moments (16) so that the solution is converged. The reference solution is taken from Peterson et al. (2022). Gamma–GQMOM and QMOM converge to the same solution, whereas lognormal–GQMOM converges to another one, closer to, but still different, from the reference solution. For Cases 1 and 2, the number N of quadrature points for GQMOM has no influence on the solution as soon as it is greater that n, which is the number of quadrature points for QMOM. The convergence issue with Case 2 is due to the very long tails of the initial lognormal distribution.

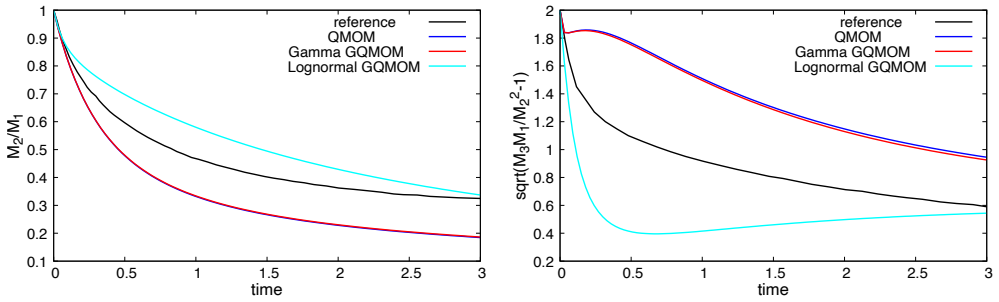

Figure 14: Fragmentation, Case 2: reference solution from Peterson et al. (2022) and converged mean (left) and variance (right) obtained for simulations with QMOM, gamma–GQMOM, and lognormal–GQMOM.

In this sense, Case 2 is an extreme case that is unlikely to occur in physical systems. Nonetheless, using lognormal–GQMOM improved the results, and it would also possible to define a GQMOM closure with even longer tails to handle such cases. In real-world applications, GQMOM provides more flexibility than QMOM to accommodate for the shape of the NDF.

5. Discussion and conclusions

In this work, we have generalized the widely used moment closure QMOM for solving moment systems derived from a 1-D PBE to allow for an arbitrarily large number N of Gauss quadrature nodes. Like QMOM does for $\mathbf{M}_{2n-1}$, GQMOM exactly reproduces the input moment vector $\mathbf{M}_{2n}$ where $2n$ is the order of the highest-order known moment. Unlike QMOM, GQMOM closes the higher-order moments such that the moment vector $\mathbf{M}_{2N}$ is (almost always) in the interior of moment space, i.e., the moments correspond to a continuous NDF unless M_{2n} is on the boundary of moment space. When the latter occurs, the GQMOM quadrature is the same as the one found with QMOM. This is because, by construction, unless $b_n = 0$, GQMOM will never produce a set of recurrence coefficients on the boundary of moment space. As we have shown through examples, the principal advantage of using GQMOM versus QMOM is the ability to increase the number of quadrature points from n to N without solving for more moments. This allows for a more accurate evaluation of the moment source terms at nearly the same computation cost. Nonetheless, as shown in the examples, the overall accuracy of the moment method is controlled principally by n (i.e., by the number of solved moments), and, hence, a much larger N is only needed for "difficult" source terms.

In comparison to other moment closures based on a continuous NDF (e.g., EQMOM, EM, EQ), GQMOM is much easier to implement because it only requires a straightforward modification of the Chebyshev algorithm to compute the additional recurrence coefficients (i.e., a_i, b_i for $i = n, n+1, \ldots, N$). Furthermore, because this process results in a Gauss quadrature on the support $\mathbb{B}$, we are guaranteed that the abscissae, being the roots of a monic orthogonal polynomial, lie inside $\mathbb{B}$ and are distinct. This is not the case, for example, with EQMOM where the abscissae from the secondary quadrature can overlap, which causes severe problems, for example, when one attempts to find conditional moments (Cheng et al., 2010; Yuan and Fox, 2011). Moreover, the weights of the Gauss quadrature from GQMOM will be positive as long as $\mathbf{M}_{2n}$ lies in the interior of moment space; otherwise, some weights will be null.

In general, moment closures that reside in the interior of moment space are preferable because they can tolerate small numerical errors without becoming non-realizable. For example, for a PBE that includes spatial transport with a known velocity (e.g., the gas velocity for an aerosol), constructing realizable finite-volume schemes is challenging (Wright, 2007), even if some realizable second-order schemes were developed (Laurent and Nguyen, 2017; Marchisio and Fox, 2013; Passalacqua et al., 2020; Shiea et al., 2020; Vikas et al., 2011). In this respect, GQMOM may allow for use of higher-order spatial reconstruction of the moment vector for cases where QMOM is limited to low order. The same issue is faced when solving the moment source terms numerically (Nguyen et al., 2016), so that, generally speaking, we expect that GQMOM will generate more robust, and more accurate, numerical solvers for the multi-scale, multi-physics codes used in

real-world applications (Bryngelson et al., 2020; Heylmun et al., 2021, 2019; Ilgun et al., 2021; Passalacqua et al., 2018; Wick et al., 2017).

Many real-world applications are described by a NDF with more than one internal variable (e.g., for aerosols, the droplet volume, temperature, composition, etc.). It is well known that the numerical solution of a multi-dimensional PBE, even for spatially homogeneous cases, is very challenging due to the high dimension of the phase space. One possible simplification is to condition the internal variables on the variable with the largest variance (Marchisio and Fox, 2013; Yuan and Fox, 2011). In applications involving droplets (aerosols), solid particles or bubbles, the mass (or size) of the particle is very often the most important internal variable. As done in the examples in section 4, GQMOM can be applied with the moments $\mathbf{M}_{2n}$ of the size variable ξ. Then, the conditional mean of another variable ϕ given ξ is denoted by $\langle\phi|\xi\rangle$, and is computed using the joint moments $\langle\phi\xi^k\rangle$ for $k = 0, 1, \ldots, n-1$ by applying the conditional quadrature method of moments (CQMOM) (Cheng et al., 2010; Yuan and Fox, 2011). Mathematically, the linear system in CQMOM is well conditioned because the QMOM abscissae are the roots of an orthogonal polynomial; thus, the same will be true for GQMOM. As with CQMOM, when QMOM is replaced by GQMOM, it will be necessary to approximate $\langle\phi|\xi\rangle$ using a set of joint moments. However, the straightforward application of CQMOM with $N > n$ abscissae yields an under-determined linear system when $k = 0, 1, \ldots, n-1$. Thus, one can either increase of order of the joint moments as to have N constraints, or modify CQMOM to handle $N > n$ abscissae. The latter can be done successfully using an interpolation function, and we will describe the resulting algorithm for generalized CQMOM in a future publication.

Declaration of competing interest

The authors declare that they have no known competing interests or personal relationships that could have appeared to influence the work reported in this paper.

Appendix A. Calculation of integrals with EQMOM

Differently from QMOM and GQMOM, in EQMOM the NDF is approximated as a weighted sum of non-negative KDF (Yuan et al., 2012):

$$f(\xi) \approx p_n(\xi) = \sum_{\alpha=1}^{n} w_\alpha \delta_\sigma(\xi, \xi_\alpha) \tag{A.1}$$

where w_α are the weights of each KDF $\delta_\sigma(\xi, \xi_\alpha)$ with standard deviation σ, ξ_α are the corresponding abscissae, and n is the number of KDF being used. Based on this approximation, integrals involving products of the NDF and a function of ξ are approximated as (Madadi-Kandjani and Passalacqua, 2015)

$$\int_0^\infty g(\xi) p_n(\xi)\,\mathrm{d}\xi = \int_0^\infty g(\xi) \sum_{\alpha=1}^{n} w_\alpha \delta_\sigma(\xi, \xi_\alpha)\,\mathrm{d}\xi = \sum_{\alpha=1}^{n}\sum_{\beta=1}^{N_\alpha} w_\alpha w_{\alpha\beta} g(\xi_{\alpha\beta}). \tag{A.2}$$

where, for fixed α, $w_{\alpha\beta}$ and $\xi_{\alpha\beta}$ are the N_α Gaussian quadrature nodes corresponding to the KDF (Yuan et al., 2012). In principle, N_α can be different for each α, but here we let $N_\alpha = 2n$.

Consequently, the evolution equation of the moment M_k in aggregation and breakup processes discussed in section 4.2 is rewritten as

$$\begin{aligned}\frac{dM_k}{dt} = {} & \frac{1}{2}\sum_{\alpha_1=1}^{n}\sum_{\beta_1=1}^{N_\alpha} w_{\alpha_1} w_{\alpha_1\beta_1} \sum_{\alpha_2=1}^{n}\sum_{\beta_2=1}^{N_\alpha} w_{\alpha_2} w_{\alpha_2\beta_2} (\xi_{\alpha_1\beta_1}^3 + \xi_{\alpha_2\beta_2}^3)^{k/3} \beta_{\alpha_1\beta_1\alpha_2\beta_2} \\ & - \sum_{\alpha_1=1}^{n}\sum_{\beta_1=1}^{N_\alpha} w_\alpha \xi_{\alpha_1\beta_1}^k w_{\alpha_1} w_{\alpha_1\beta_1} \sum_{\alpha_2=1}^{n}\sum_{\beta_2=1}^{N_\alpha} w_{\alpha_2} w_{\alpha_2\beta_2} \beta_{\alpha_1\beta_1\alpha_2\beta_2} \\ & + \sum_{\alpha=1}^{n}\sum_{\beta=1}^{N_\alpha} w_\alpha a_{\alpha\beta} \bar{b}_{\alpha\beta}^k w_{\alpha\beta} - \sum_{\alpha=1}^{n}\sum_{\beta=1}^{N_\alpha} w_\alpha \xi_{\alpha\beta}^k a_{\alpha\beta} w_{\alpha\beta}\end{aligned} \tag{A.3}$$

where $\bar{b}^k_{\alpha\beta} = \bar{b}^k(\xi_{\alpha\beta})$. In the numerical implementation of EQMOM, σ is found from M_{2n} using an iterative procedure (Pigou et al., 2018; Yuan et al., 2012). Thus, since $N \approx nN_\alpha$, the principal advantage of GQMOM versus EQMOM is to eliminate the need for iterations to find σ before evaluating the right-hand side of eq. (A.3).

References

Böhmer, N., Torrilhon, M., 2020. Entropic quadrature for moment approximations of the Boltzmann–BGK equation. Journal of Computational Physics 401, 108992. URL: http://www.sciencedirect.com/science/article/pii/S0021999119306977, doi:https://doi.org/10.1016/j.jcp.2019.108992.

Bryngelson, S.H., Colonius, T., Fox, R.O., 2020. QBMMLib: A library of quadrature-based moment methods. SoftwareX 12, 100615.

Cheng, J.C., Vigil, R.D., Fox, R.O., 2010. A competitive aggregation model for flash nanoprecipitation. J. Colloid Interface Sci. 351, 330–342.

Dette, H., Studden, W.J., 1997. The Theory of Canonical Moments with Applications in Statistics, Probability, and Analysis. Wiley Series in Probability and Statistics: Applied Probability and Statistics, John Wiley & Sons Inc., New York.

Fox, R.O., Laurent, F., 2022. Hyperbolic quadrature method of moments for the one-dimensional kinetic equation. SIAM J. Appl. Math. 82, 750–771.

Gautschi, W., 2004. Orthogonal Polynomials: Computation and Approximation. Oxford University Press, Oxford, UK.

Gautschi, W., Li, S., 1991. Gauss–Radau and Gauss–Labatto quadratures with double end points. Journal of Computational and Applied Mathematics 34, 343–360.

Grosch, R., Briesen, H., Marquardt, W., Wulkow, M., 2007. Generalization and numerical investigation of QMOM. AIChE Journal 53, 207–227.

Hamburger, H.L., 1944. Hermitian transformations of deficiency-index (1,1), Jacobian matrices, and undetermined moment problems. Amer. J. Math. 66, 489–552.

Heylmun, J.C., Fox, R.O., Passalacqua, A., 2021. A quadrature-based moment method for the evolution of the joint size–velocity number density function of a particle population. Computer Physics Communications 267, 108072.

Heylmun, J.C., Kong, B., Passalacqua, A., Fox, R.O., 2019. A quadrature-based moment method for polydisperse bubbly flows. Computer Physics Communications 244, 187–204.

Ilgun, A.D., Fox, R.O., Passalacqua, A., 2021. Solution of the first-order conditional moment closure for multiphase reacting flows using quadrature-based moment methods. Chemical Engineering Journal 405.

Jaynes, E.T., 1957. Information theory and statistical mechanics. The Physical Review 106, 620–630.

Lage, P.L., 2011. On the representation of QMOM as a weighted-residual method – the dual-quadrature method of generalized moments. Computers and Chemical Engineering 35, 2186–2203.

Laurent, F., Nguyen, T.T., 2017. Realizable second-order finite-volume schemes for the advection of moment sets of the particle size distribution. Journal of Computational Physics 337, 309–338.

Madadi-Kandjani, E., Passalacqua, A., 2015. An extended quadrature-based moment method with log-normal kernel density functions. Chemical Engineering Science 131, 323–339.

Marchisio, D.L., Fox, R.O., 2013. Computational Models for Polydisperse Particulate and Multiphase Systems. Cambridge University Press, Cambridge, UK.

Marchisio, D.L., Pikturna, J.T., Fox, R.O., Vigil, R.D., 2003. Quadrature method of moments for population-balance equations. AIChE Journal 49, 1266–1276.

McGraw, R., 1997. Description of aerosol dynamics by the quadrature method of moments. Aerosol Science and Technology 27, 255–265.

McGraw, R., Merry, G.A., 1985. Excitation transfer in disordered systems: Bounds on the decay of donor excitation. Chemical Physics 96, 97–108.

McGraw, R., Nemesure, S., Schwartz, S.E., 1998. Properties and evolution of aerosols with size distributions having identical moments. J. Aerosol Sci. 29, 761–772.

Mead, L.R., Papanicolaou, N., 1984. Maximum entropy in the problem of moments. J. Math. Phys. 25, 2404–2417.

Nguyen, T.T., Laurent, F., Fox, R.O., Massot, M., 2016. Solution of population balance equations in applications with fine particles: mathematical modeling and numerical schemes. Journal of Computational Physics 325, 129–156.

Passalacqua, A., Laurent, F., Fox, R.O., 2020. A second-order realizable scheme for moment advection on unstructured grids. Computer Physics Communications 248, 106993.

Passalacqua, A., Laurent, F., Madadi-Kandjani, E., Heylmun, J.C., Fox, R.O., 2018. An open-source quadrature-based population balance solver for OpenFOAM. Chemical Engineering Science 176, 306–318.

Peterson, J.D., Bagkeris, I., Michael, V., 2022. A new framework for numerical modeling of population balance equations: Solving for the inverse cumulative distribution function. Chemical Engineering Science 259, 117781.

Pigou, M., Morchain, J., Fede, P., Penet, M.I., Laronze, G., 2018. New developments of the extended quadrature method of moments to solve population balance equations. Journal of Computational Physics 365, 243–268.

Randolph, A.D., Larson, M.A., 1988. Theory of Particulate Processes: Analysis and Techniques of Continuous Crystallization. Academic Press.

Schmüdgen, K., 2017. The Moment Problem. volume 277 of *Graduate Texts in Mathematics*. Springer, Cham.

Shiea, M., Buffo, A., Vanni, M., Marchisio, D.L., 2020. A novel finite-volume TVD scheme to overcome non-realizability problem in quadrature-based moment methods. Journal of Computational Physics 409, 109337.

Vanni, M., 2000. Approximate population balance equations for aggregation–breakage processes. J. Colloid Interface Sci. 221, 143–160.
Vikas, V., Wang, Z.J., Passalacqua, A., Fox, R.O., 2011. Realizable high-order finite-volume schemes for quadrature-based moment methods. J. Comput. Phys. 230, 5328–5352.
Wheeler, J.C., 1974. Modified moments and Gaussian quadratures. Rocky Mt. J. Math. 4, 287–296.
Wick, A., Nguyen, T.T., Laurent, F., Fox, R.O., Pitsch, H., 2017. Modeling soot oxidation with the extended quadrature method of moments. Proceedings of the Combustion Institute 36, 789–797.
Wilck, M., 2001. A general approximation method for solving integrals containing a lognormal weighting function. J. Aerosol Sci. 32, 1111–1116.
Wright, D.L., 2007. Numerical advection of moments of the particle size distribution in Eulerian models. J. Aerosol Sci. 38, 352–369.
Yuan, C., Fox, R.O., 2011. Conditional quadrature method of moments for kinetic equations. J. Comput. Phys. 230, 8216–8246.
Yuan, C., Laurent, F., Fox, R.O., 2012. An extended quadrature method of moments for population balance equations. J. Aerosol Sci. 51, 1–23.